ELSEVIER

International Journal of Mass Spectrometry 205 (2001) 309–323

International Journal of Mass Spectrometry

Studies of low-energy electron attachment at surfaces

A.A. Tuinman[a], A.S. Lahamer[b], R.N. Compton[a,c,*]

[a]*Department of Chemistry, The University of Tennessee, Knoxville, TN 37996*
[b]*Department of Physics, Berea College, Berea, KY 40404*
[c]*Department of Physics, The University of Tennessee, Knoxville, TN 37996*

Received 1 March 2000; accepted 2 May 2000

Abstract

Studies of the formation of negative ions at heated metal surfaces are reported under two experimental conditions: (1) laser desorption/ablation ionization and (2) heated metal wires in the presence of fluorine gas. In condition (1), nanoclusters of boron nitride/graphite are first produced by laser ablation of boron nitride mixed with graphite in a heated (~1100 °C) rare gas followed by laser desorption negative ionization to yield a wide variety of cluster anions. The negative ion mass spectra for laser ablation/desorption ionization of small cluster ions from fullerenes, graphite, or most carbon containing metals (e.g. stainless steel) show common features (C_n^- for $n = 1$ to ~10, with even > odd alternation). The laser serves to heat the surface, produce clusters, and provides free and "quasifree" electrons for attachment and to dissociate larger negative ions/neutrals to produce low-mass cluster anions. Laser desorption of $C_{60}H_{36}$ and $C_{60}F_{48}$ at high laser power results in intense H^- and F^- ion signals, respectively. In the case of $C_{60}H_{36}$, the H^- ion production is attributed to dissociative electron attachment, i.e. $e + C_{60}H_{36} \rightarrow C_{60}H_{35} + H^-$. For the case of $C_{60}F_{48}$, both dissociative attachment and photodissociation of $C_{60}F_{48}^-$ are believed responsible for the F^- ion yield. These observations form the basis for the development of intense pulsed ion sources of H^- and F^- ions for use in energy production (fuel injection into fusion reactors), spallation neutron devices, lithography, and other applications. In condition (2), heated metal wires of Al, Au, Au/Pd, Nb, Ni/Cr, Pt, Re, Ta, Ti, V, W, and Zr are "burned" in a low pressure vapor of fluorine gas (~10^{-4} Torr) resulting in a wide variety of molecular anions (e.g. $Al_2F_9^-$; $AuF_{2,3}^-$; NbF_6^-; $ReF_{5,6}^-$; TaF_6^-; $Ti_{4,5}^-$; $VF_{4,5}^-$; $WF_{5,6}^-$; ZrF_5^-, and $Zr_2F_9^-$) of varying intensity. Also of interest are the occurrences of F_3^- and the "impurity" ion $Na_2F_3^-$. (Int J Mass Spectrom 205 (2001) 309–323) © 2001 Elsevier Science B.V.

Keywords: Electron attachment; Surface ionization; Laser desorption ionization; Electron affinities; TOF mass spectrometry

1. Introduction

The formation of negative ions on surfaces has been studied under a large range of experimental conditions. Negative surface ionization [1] is probably the best studied of these processes where a molecule accommodates itself on a "hot" surface, picks up an extra electron from the Fermi sea of electrons and leaves the surface as an anion. Measurements of the ion yield as a function of surface temperature has provided information on the difference in work function of the surface and the binding energy of the anion (i.e. electron affinity). In a related study [2], surface reaction negative ionization was also reported in which the "burning" of uranium wires in fluorine gas was found to produce very large

* Corresponding author. E-mail: rcomplon@utk.edu

Dedicated to Professor Aleksandar Stamatovic on the occasion of his 60th birthday.

PII S1387-3806(00)00276-1

currents (microampere beams) of UF_6^- negative ions. Although the processes leading to the formation of negative ions is not well understood, surface ionization is presumably the final step.

Recent attention has turned to negative ion formation via low-energy electron interactions with solids. Sanche [3] has reviewed the progress in this relatively new field of research; electron stimulated desorption ionization. Likewise, laser desorption negative ionization mass spectroscopy represents an important new tool in materials analysis characterization and mass spectroscopy of biomaterials. The use of so-called matrix assisted laser desorption ionization also allows for desorption ionization with minimum fragmentation. Despite its increasing importance, the mechanisms leading to laser desorption negative ionization are not well understood at the present time. One can postulate that both surface ionization as well as free or quasifree electron attachment (i.e. electron stimulated desorption) would be important. The present study represents an experimental investigation of laser desorption negative ionization of nanoclusters as well as a full account of the formation of negative ions from burning wires in fluorine gas.

2. Experimental

2.1. Laser desorption time-of-flight mass spectrometry experiments

The negative ions were analyzed using a laser desorption/ionization time-of-flight (TOF) mass spectrometer as previously described [4]. The experimental arrangement consists of the following elements: a sample probe in the sample chamber, accelerating electrodes, ion flight tube, microchannel plate detectors and data recording system, ion-focusing system, LN1000-nitrogen laser system and a series of microscope slides for attenuation of the laser beam. The whole system was operated under a high vacuum (10^{-8} Torr). A layer of sample is deposited on the "tip" of the probe by evaporation from solution or vacuum sublimation. The laser beam (e.g. LN1000-nitrogen laser with wavelength of 337.1 nm and a 600 ps duration) is mildly focused onto the sample. When the laser beam impinges on the sample, molecules are ejected from the surface into the gas phase, along with positive/negative ions. In addition, electrons are ejected into the gas phase which can also attach to gas phase molecules. A photodiode near the laser beam is used to pick up the pulse signal as a start trigger. The arrival time spectra (0–100 μs) are recorded by a digital oscilloscope and converted to ion mass distributions. The laser beam power density is varied in two ways: either a set of microscope slides is introduced to act as a beam attenuator, or the focal point of the laser beam is adjusted to a different distance. Usually the laser was focused to a point beyond the sample. The sample probe tips are made from Cu, stainless steel (ss), or Ta metals. Most of the samples are prepared in a toluene solvent before drying on the tips. In order to confirm the results, other solvents (e.g. tetrahydrofuran etc.) are also used. The calibration of mass spectra is often determined from well known masses which exist in the spectra (e.g. Na^+, K^+, Cl^-, C_{60}^-, etc.). In some difficult cases, e.g. $C_{60}H_{36}$, adding a small amount of C_{60} or C_{70} to the sample is very helpful for mass calibration purposes.

Samples of $C_{60}H_{36}$ were prepared by three different methods; (1) direct exposure of fullerene to high pressure hydrogen, (2) catalytic reduction of fullerenes in solution with a platinum oxide catalyst [5], and (3) a process using Zn and conc. HCl [6]. Samples of $C_{60}F_{48}$ were prepared using a direct fluorination of C_{60} at 250 °C in a sodium fluorine matrix [7]. Nanoclusters of mixed (2:1) boron nitride/graphite (BNC) were synthesized using modifications of a technique developed by Smalley and co-workers [8] for the production of endohedral fullerenes and carbon nanotubes. Our adaptation of the method of Smalley and co-workers has been fully described [9].

2.2. In situ reaction of metal wires with fluorine within a magnetic sector mass spectometer

The metal-wire/fluorine-gas "combustion" analyses were conducted on a hybrid mass spectrometer of BEqQ geometry; the ZAB-EQ from VG-Analytical (Manchester, England). Portions of the instrument

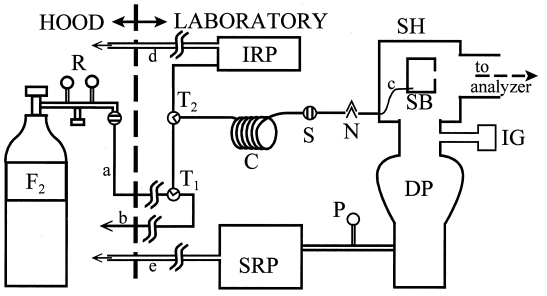

Fig. 1. Schematic diagram of the gas train for safe introduction of highly reactive and toxic elementary fluorine to the source block of the ZAB mass spectrometer. All components are stainless steel, and all tubing is 1/8 in., except as indicated below. A cylinder of fluorine gas (F_2) with a pacified pressure regulator (R) is kept in a well ventilated fume hood. Tubes (a, b) lead to and from the ZAB, where three-way valves (T1, T2) direct the flow of a "plug" of F_2 at 1 atm. to a 1/4 in. diameter expansion coil (C) where the pressure is reduced ~100-fold. A shutoff valve (S) and a needle valve (N) allow regulation of flow to the ion-source block (SB) via a teflon capillary (c). To protect the hot filament of the Bayard-Alpert ion gauge (IG) during this mode of operation, the gauge is switched off and source housing pressure is monitored indirectly at the Pirani gauge (P) situated between the diffusion pump (DP) and its backing rotary pump (SRP). The ZAB's inlet's rotary pump (IRP) allows evacuation of the expansion coil C through valve T_2 when required. The exhaust tubes (d, e) of the rotary pumps are large diameter Tygon.

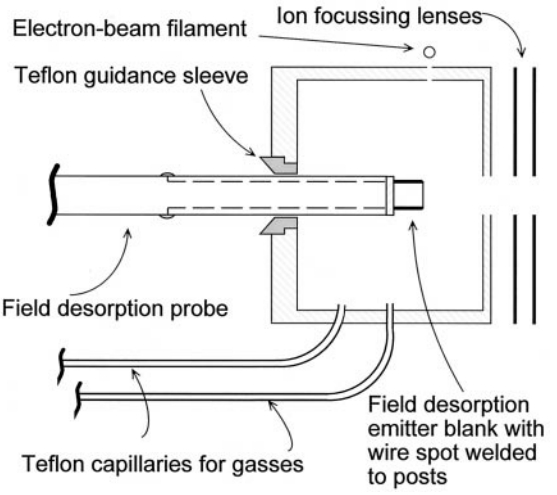

Fig. 2. The ion-source block for combustion of metals in F_2 in the ZAB mass spectrometer. A Teflon sleeve at the rear of the source guides the field desorption (FD) probe with minimum clearance (<0.5 mm) to maintain a high pressure differential between the inside and outside of the block when gas is introduced via a Teflon capillary. The FD probe carries an FD-emitter blank to which is spot welded a piece (~4 mm) of the wire under investigation. Heating current to the wire is provided via the standard contact points of the FD probe. Elementary fluorine is introduced via a Teflon capillary. The ion source is further equipped with a filament assembly and a second capillary, the combination of which allowed operation in the negative-ion chemical ionization mode to enable calibration of magnet scans.

were specially adapted for these experiments. Thus, a gas train was constructed to allow the controlled introduction of F_2 into the ion source (see Fig. 1). Because there is no direct pressure measurement within the source block, the operative pressure is estimated from the readings at the Pirani gauge. Despite numerous experiments consuming significant amounts of highly reactive F_2 gas, no detrimental effects were noted on the ion source, source housing, or vacuum pumps. A dedicated ion source was also constructed for this project, based loosely on the standard ZAB field desorption ion source (see Fig. 2). In order to provide the high currents needed to effectively heat short lengths of low resistance wire (e.g. 4 mm of 250 μm Au wire) a 50 A 12 V auto battery was connected to solid-state circuitry to allow voltage control of the output. The battery and circuitry were encased in an electrically insulating plexiglass box so that the entire assembly could be "floated up" to the accelerating voltage of the ZAB (8 kV). The output of the battery was connected through existing feed throughs on the flange of the source housing to provide the necessary current (up to 10 A) to the wire being analyzed.

In a typical experiment, the wire was introduced into the ion source via the vacuum lock of the ZAB, F_2 gas was introduced as depicted in the caption to Fig. 1, scanning of the magnetic sector was commenced, and heating current was supplied to the wire by adjusting the potentiometer control of the 12 V external battery power supply. The heating current was increased stepwise at periodic intervals whereas the acquired spectra were monitored in "real-time" with the OPUS data system. In most cases total ion currents of the spectra were extremely low initially, but experienced a sudden increase at a specific heating-current voltage. At that point the stepwise increase in heating current was halted, but spectral acquisition continued. The reaction usually proceeded

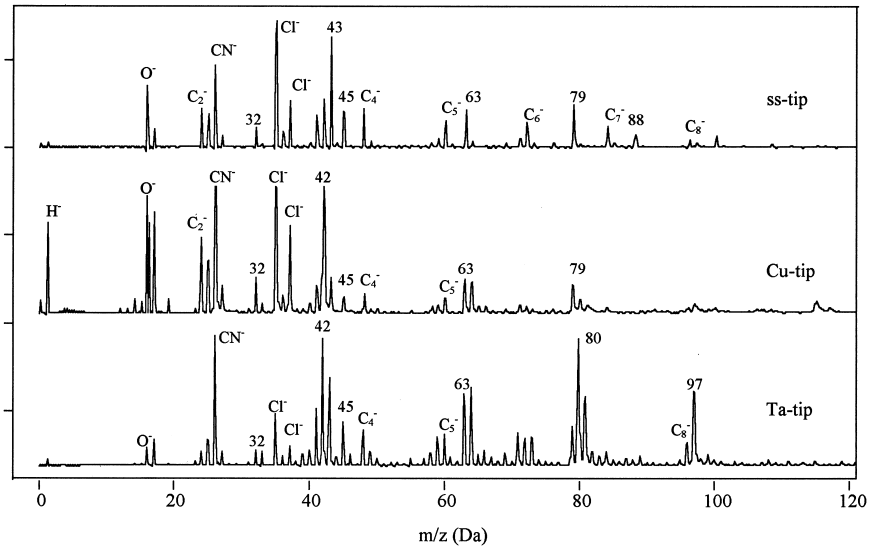

Fig. 3. Negative ion TOF mass spectra of bare metal sample tips. *m/z* 24, 36, 48, . . . are attributed to C_n^-, n = 2, 3, 4, . . . , respectively. These mass peaks are most prominent in the ss tip. Other common *m/z* among the tips are 26 (CN^-) and 35/37 (Cl^-).

to completion (breaking/melting of the wire) at the same voltage. Visual monitoring of the wire temperature (observation of the color of reflected light from the wire visible through the glass window of the source housing on the ZAB) indicated an ever increasing temperature (dull red → cherry red → white) at the same voltage. This is explained by the increase in wire resistance as its diameter is decreased by depletion of the metal surface through reaction with fluorine. Termination of the reaction took anywhere from

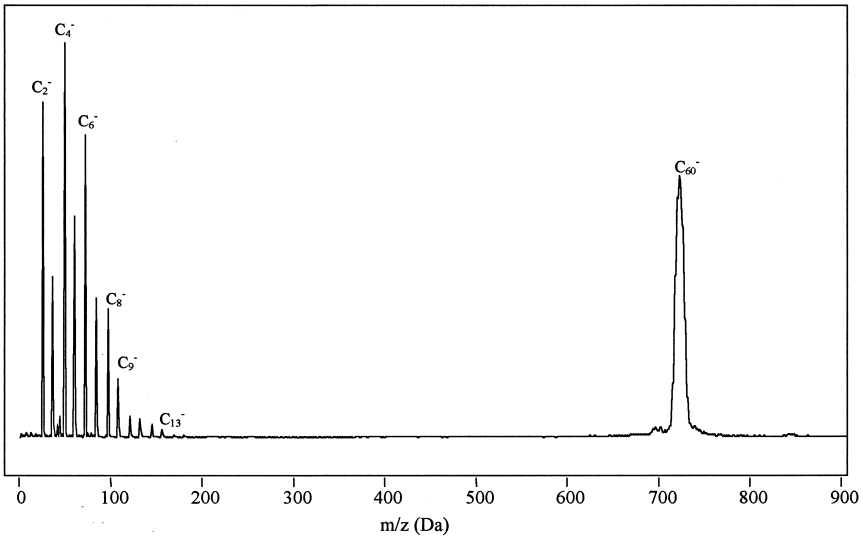

Fig. 4. Negative ion TOF mass spectrum of C_{60} on a Ta tip. Abundant *m/z* of 24, 36, 48, . . . , 156, are attributed to C_n^- (n = 2, 3, 4, . . . , 13) respectively. TOF mass spectra of C_{60} are the same for Ta, ss, and Cu tips.

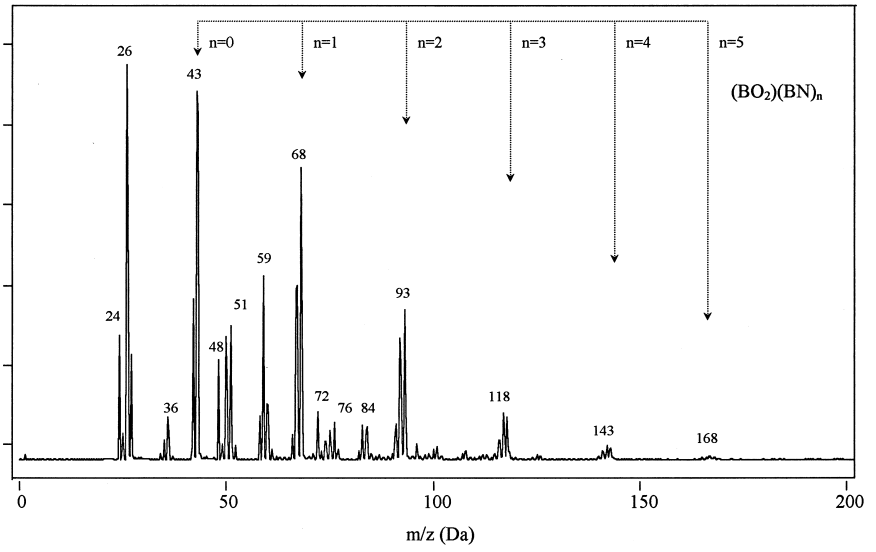

Fig. 5. Negative ion TOF mass spectrum of BNC material on a ss tip. All peaks are identified. The series *m/z* 43, 68, 93, 118, 143, and 168 is attributed to $(BO_2)(BN)_n^-$ (n = 0–5). The series *m/z* 26, 51, 76, and 101 is assigned to $CN(BN)_n^-$ (n = 0–3). The series *m/z* 35, 47, 59, 71, and 83 corresponds to C_nB^- (n = 2–6). Observed intensities are in agreement with the theoretical isotopic mass distributions. C_n^- ($n \leq 9$) is also present.

tens of seconds to several minutes, depending *inter alia* on the melting point of the metal. As the wire temperature increased, the relative intensities of observed peaks in spectra sometimes changed also.

In these experiments determination of "accurate masses" (i.e. <2 ppm deviation from theoretical) is not possible because of the lack of suitable reference materials which produce closely spaced peaks of known elementary composition under the conditions of the experiment. Mass calibrations were made in a separate electron capture experiment utilizing the electron beam capability of the ion source (see Fig. 2) with reference materials such as chloroform and trifluoroacetic acid. The present mass assignments are thought to be accurate within ~0.07 Da, based on comparison of the observed masses of ions identified by their isotope cluster shape with the calculated (theoretical) masses of those ions.

3. Results and discussion

In our initial studies of laser desorption negative ionization (LDNI) we examined the LD from metal sample "tips" made of stainless steel, tantalum, and copper. Fig. 3 shows the results of these studies for laser powers sufficient to observe the anions. We stress that these powers are generally larger than those required to observe ions when samples are deposited on the tips. We have tentatively identified many of the anions in Fig. 3. Of particular interest is the formation of C_n^- ions from ss. Other "impurity" peaks are also detected, such as CN^- and Cl^-. LDNI mass spectra for the copper and tantalum tips also show a large number of ion peaks many of which are common to ss. By comparison, Fig. 4 shows the LDNI data for a C_{60} covering on Ta. Here the signals are much larger and all peaks are attributed to C_n^- with n = 2 to ~13 including a large peak at C_{60}^-. The same features were observed for C_{60} on Cu and ss substrates. The C_{60}^- signal is attributed to both free electron attachment (from electrons produced by laser ejection and thermionic emission) and surface ionization. Free electron attachment to the carbon cage C_{60} fullerene molecule has been studied in cross beam experiments [10–13] and with flowing afterglow/Langmuir probe FLAP [14] techniques. These studies reveal a most unusual

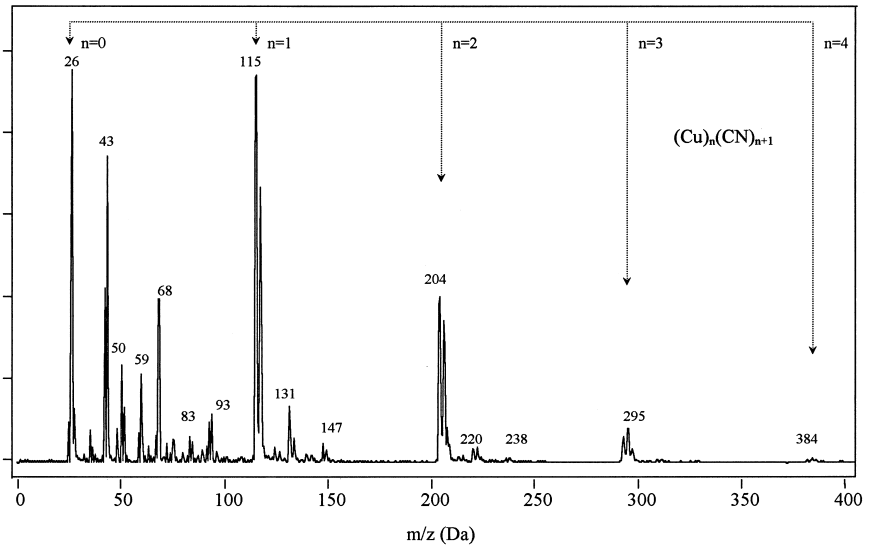

Fig. 6. Negative ion TOF mass spectrum of BNC sublimed on a Cu tip. All peaks are identified. The series *m/z* 25, 50, 75, and 100 corresponds to $(BN)_n^-$ (n = 1–4). The series *m/z* 26, 115, 204, 295, and 384 is attributed to $(Cu)_n(CN)_{n+1}^-$ (n = 0–4). The series *m/z* 35, 59, 83, 107, and 131 is assigned to $(C_{2n}B)^-$ (n = 1–5). The series *m/z* 43, 68, and 93 belongs to $(BO_2)(BN)_n^-$ (n = 0–2). The series *m/z* 26, 51, 76, 101 corresponds to $(CN)(BN)_n^-$ (n = 0–3). The series *m/z* 131, 220, and 309 represents $(Cu_nO)(CN)_{n+1}^-$ (n = 1, 2, and 3). Observed intensities are in a agreement with the theoretical isotopic mass distributions.

attachment cross section behavior: a large attachment cross section is observed up to ~15 eV. In addition, some of the experiments indicate a fall off in the cross section at energies below ~0.2 eV. The fall off at low energies is consistent with the theoretical conjectures of Tosatti and Manini [15], who argue that *s*-wave attachment to C_{60} is symmetry forbidden (see also [9]). Unfortunately, the reports of the absence of *s*-wave free electron attachment to C_{60} have been refuted in two recent experimental studies [16,17]. Both of these studies report electron attachment thresholds which are coincident with that of electron attachment to SF_6 to form SF_6^- (i.e. at ~0 energy). The "zero-energy" resonance in SF_6 was used to calibrate the electron energy scale. We caution, however, that the use of this method of energy calibration requires special experimental attention. Schulz [18] was the first to point out if a very slight positive potential exists in the electron interaction region, the electrons entering this region can never reach zero energy. The result is to shift all of the higher energy features down in "nominal" energy (i.e. reading on the voltmeter used to establish the energy scale). The SF_6^- peak cannot shift below "zero" energy, however, a higher-energy peak can be shifted down to be coincident with the SF_6^- peak. These effects were also discussed in many of our earlier publications (see e.g. [19] and [20]). In the studies of Huang et al. [13], as in our earlier studies, a small bias voltage was applied to the collision chamber in order to compensate for any contact potential bias, external fields, or surface potentials which might be present. In these studies [13] it was found that a slight excess positive voltage applied to the chamber could shift the C_{60}^- peak and threshold down in energy to be coincident with that of SF_6^-. We tentatively suggest that such potentials may have been present in the studies reporting *s*-wave capture [16,17]. Further information bearing upon low-energy electron attachment to C_{60} comes from studies of high-Rydberg atom electron charge exchange reactions. Huang et al. [13] studied the reactions of high Rydberg *np* states with C_{60} for n^* = 10–43 and found a reasonably large charge exchange rate for the formation of C_{60}^-. More recent studies by Weber et al. [21] and Finch et al. [22] extend the reaction rate measurements to effective principal

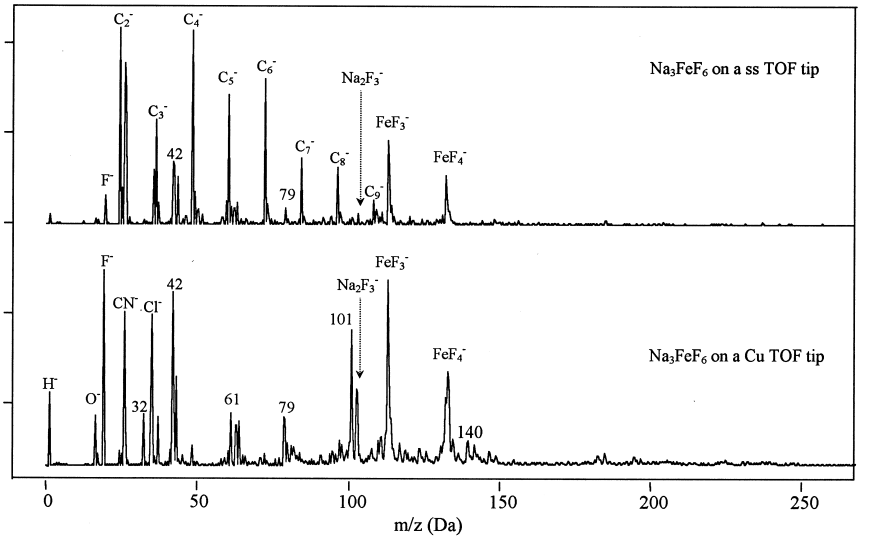

Fig. 7. Negative ion TOF mass spectra of Na_3FeF_6 on a ss and a Cu TOF tips, illustrating the role of the sample surface. The *m/z* 19, 103, 113, and 132 are assigned to F^-, $Na_2F_3^-$, FeF_3^-, and FeF_4^-, respectively. The series *m/z* 24, 36, 48, . . . , 108, corresponding to C_n^- (n = 2–9) appears only in the ss substrate spectra.

quantum numbers, n^*, well over 100. The reaction rates for high Rydberg charge transfer are expected to be equivalent to those for slow free-electron attachment. Thus, the observation of Rydberg charge transfer with C_{60} especially the relatively constant rate for n^* from ∼40 to 270 [21], appears to contradict the earlier free electron attachment data [10–13] and the theoretical predictions of no *s*-wave capture. A number of possible explanations for this discrepancy have been proposed; symmetry breaking due to the electric field of the ion core [13], rotations resulting in polar "flattening" of the molecule [22], a polarization-bound $L = 0$ state [22], and the presence of a narrow, virtual *s*-wave resonance which escapes detection in the beam experiments but is detected in the Rydberg experiments [21]. Although more studies are needed to complete this interesting story, it is important to point out that Rydberg charge transfer to the prolate C_{70} molecule exhibits an n-dependence similar to that of the C_{60} molecule [21]. Thus, the observation of Rydberg charge transfer at high n suggests that C_{60}^- in LDNI could also be formed by reactions of C_{60} with quasifree electrons (i.e. thermionic electrons which cannot escape their image charges).

The formation of low mass carbon cluster anions for n = 2–13 shown in Fig. 4 is most interesting. One could postulate that laser heating of the fullerenes on the surface produces small C_n clusters followed by electron attachment or surface ionization. Carman and Compton [23] have examined slow electron attachment (via high Rydberg charge transfer) to small carbon clusters and observe very different mass spectra. These experiments show enhanced electron attachment (high-Rydberg state charge transfer) for n = 5, 10, 12, 16, and 18. Surface ionization was not studied, however, the reactions of carbon clusters with slow ground state alkali atoms produced a mass spectrum reflecting those carbon clusters with high electron affinities (the "even-*n*-cluster" anions). The mass spectrum in Fig. 4 may represent a combination of slow electron attachment and surface ionization. However, given the propensity for C_{60} to lose C_2 upon laser excitation, the low mass C_n^- could also be a result of photodissociation of hot C_{60}^-. Much more work is necessary to fully understand the origin of the low mass C_n^- ions.

We now turn to the LDNI of the small mass clusters of the prepared sample of BNC. The laser

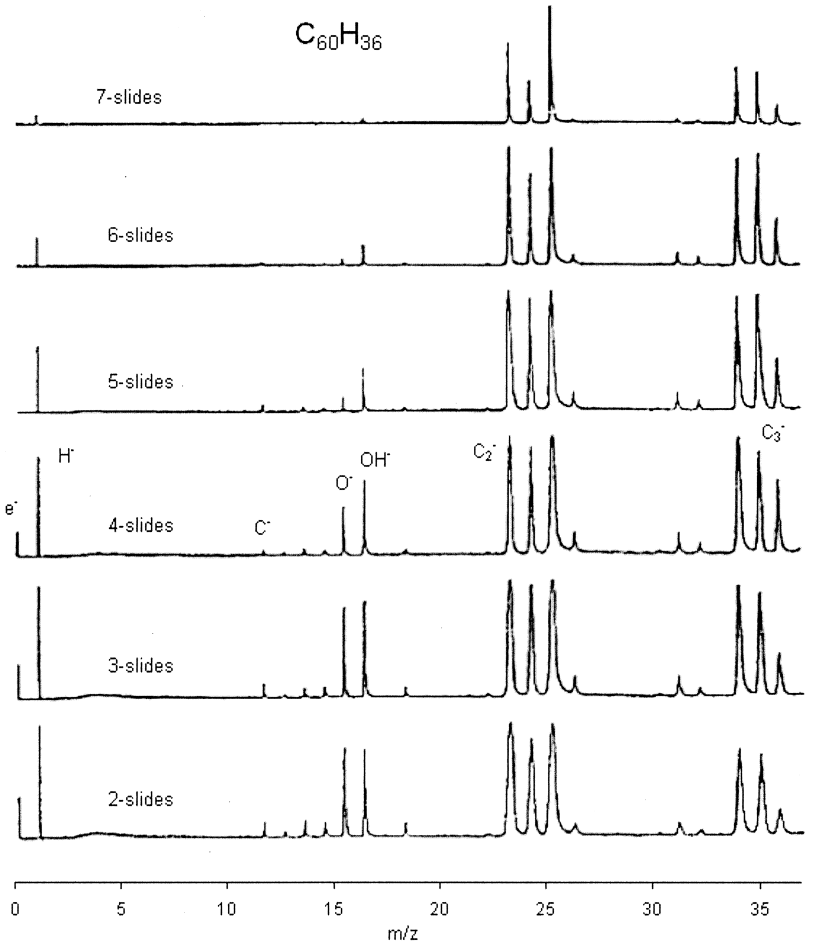

Fig. 8. Laser desorption negative ion mass spectrum for low-mass anions from $C_{60}H_{36}$. Note the occurrence of electrons (e^-) and hydrogen anions (H^-). The parameter "*n*-slides" depicts the number of microscope slides used to attenuate the laser beam (see sec. 2).

ablation material was dissolved in toluene and placed on the sample tip to dry to a surface covering. Fig. 5 shows a large variety of small negative ion clusters. Not shown is a small peak corresponding to C_{60}^-. The occurrence of $(BO_2)(BN)_n^-$ for $n = 0$–5 (clusters at *m/z* 43, 68, 91, *etc.*) suggests that reactions with air impurities changed the surface composition before analysis. The effects of the metal substrate is seen in Fig. 6 where the laser ablation products have been deposited on a copper surface and analyzed by LDNI. Many of the ions seen in this spectrum are common to those for the ss tip, however there are strong peaks corresponding to $(Cu)_n(CN)_{n+1}^-$ for $n = 1$–5. Thus it is obvious that the composition of the sample tip plays an important roll in the anionic products. We provide one final example of the effects of the sample surface for the case of Na_3FeF_6 on a ss and Cu tip. The Na_3FeF_6 was first dissolved in C_6F_6 and placed on the tips to dry. Fig. 7 shows a variety of mass peaks common to both ss and Cu including FeF_3^-, FeF_4^-, and $Na_2F_3^-$ (*m/z* 113, 132, and 103, respectively).

3.1. Intense H^- beams by laser desorption of $C_{60}H_x$

The mass range of LD positive ion peaks for $C_{60}H_{36}$ usually extend from 720 to 756 due to the

thermal decomposition into $C_{60}H_x^+$ ($x \leq 36$). The laser desorption negative ion mass spectra for $C_{60}H_{36}$ found in this work and reported previously [5] show only negative ions of $C_{60}H_x$ for $x = 1$ to ~10 with the ion intensity decreasing rapidly from $x = 1$ to $x = 10$. This observation is consistent with theoretical predictions of the electron affinities (EA) for $C_{60}H_x$ (see [4] and [5]).

Fig. 8 shows the negative ion mass spectra at low mass for various laser powers for $C_{60}H_{36}$ deposited on a copper substrate. Of particular interest is the occurrence of H^- ions along with a signal corresponding to electrons. The peak near mass zero (~0.0005 Da) is identified as electrons based upon the TOF, as well as through the observation that a small permanent magnet placed close to the flight tube extinguished this signal leaving the H^- undiminished. We can speculate about the mechanism leading to the relatively large H^- ion yield. The cross section for electron attachment to C_{60} forming long-lived C_{60}^- anions is large and extends from ~0 to ~15 eV as discussed above. If we assume that electrons can attach to $C_{60}H_{36}$ over this approximate energy range, the final product would be $C_{60}H_x^-$ ($x \leq 10$) and H^-. Any $C_{60}H_x^-$ ions in the laser field might also undergo photodissociation to produce H^- ions. The H^- ion signal at reasonable laser intensity is much greater than that for $C_{60}H_x^-$, thus the primary ionization process observed is believed to be dissociative electron attachment

$$e + C_{60}H_{36} \rightarrow C_{60}H_{36}^-{}^* \rightarrow [C_{60}H_x + y\,H] + H^- \qquad (x + y = 35). \tag{1}$$

This observation prompts the suggestion that laser ablation of hydrogenated fullerenes or perhaps hydrogenated carbon nano-tubes on a surface would allow the development of a bright source of H^- ions.

Atomic negative ions of hydrogen are used in many areas of science and technology relating to energy production and fundamental research. Intense H^- ion sources are needed to produce neutral beams for fuel injection into the next-generation magnetic fusion devices [24]. One fundamental study using H^- is that performed on the reactions of antiprotons with H^- to form protonium [25]. There are also proposals to accelerate H^- ions into synchrotrons for medical applications [26]. The current spallation neutron devices at the Ratherford Laboratory and the SNS under construction at the Oak Ridge National Laboratory by the DOE) rely upon H^- ion sources [27]. These and many other uses of H^- negative ion sources in particle accelerators have been reviewed by Dinov [28].

The H^- ion source proposed herein offers a number of potential advantages: (1) high intensity pulsed operation with controllable repetition rate; (2) minimum gas loading to vacuum system; (3) the ion source requires no electron beam, thereby simplifying the high voltage and other requirements; (4) anticipated long lifetime of the source. The last advantage cited does require a mechanism for continuous exposure of the pulsed ion beam to new hydrogenated fullerenes.

3.2. Intense F^- beams by laser desorption of $C_{60}F_{48}$

Laser desorption mass spectrometry of $C_{60}F_{48}$ to produce $C_{60}F_x^-$ has been reported previously. Here we focus on the production of F^- ions as shown in Fig. 9. Note also the formation of C_n^- ions reminiscent of that shown in Fig. 4 for C_{60} covered surfaces. Thus, as in the case of H^-, we propose that laser desorption of $C_{60}F_{48}$ could provide an intense pulsed source of F^- for many applications including lithography. The F^- ion could result from both dissociative electron attachment and photodissociation

$$e + C_{60}F_{48} \rightarrow C_{60}F_{48}^-{}^* \rightarrow [C_{60}F_x + yF] + F^- \qquad (x + y = 47) \tag{2}$$

$$C_{60}F_{48}^- + h\nu \rightarrow [C_{60}F_x + yF] + F^- \qquad (x + y = 47) \tag{3}$$

3.3. Combustion of metal wires in a fluorine atmosphere

Certain metal fluorides are known to possess electron affinities which are greater than that of the

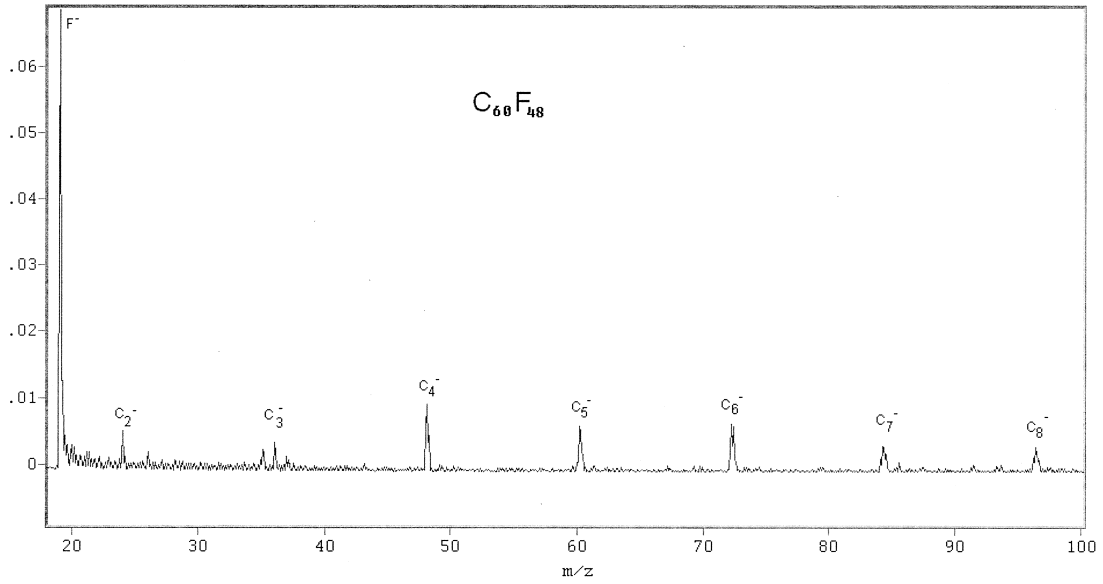

Fig. 9. Laser desorption negative ion mass spectrum of $C_{60}F_{48}$ at low mass. Note the intense F^- peak and the absence of F_2^- and F_3^-. Peaks each side of C_3^- are attributed to $^{35}Cl^-$ and $^{37}Cl^-$. Not shown is the progression $C_{60}F_{48}^-$, $C_{60}F_{48}^-$, $C_{60}F_{48}^-$, etc. at higher mass.

ionization potentials for many atoms and molecules [29,30]. The term "superhalogen" has been designated for these molecules [31,32]. For example, the electron affinities for *d*-shell metal atom hexafluorides molecules, MF_6, are estimated to vary from 5 to about 10 eV (see [30]). Gold hexafluoride is thought to possess the largest electron affinity. Bartlett [29] used a Born-Haber cycle calculation for gold fluoride salts to obtain an electron affinity of ~10.5 eV for AuF_6. Compton and Reinhardt [33] measured the center-of-mass energy onset for the formation of AuF_6^- from the reactions of fast alkali beams with beams of Au_2F_{10} (e.g. $Cs + Au_2F_{10} \rightarrow Cs^+ + AuF_6^- + AuF_4$) to deduce an electron affinity of ~10 eV for gold hexafluoride. The large electron affinity of these hexaflouride molecules can be attributed to (1) their nonbonding highest occupied molecular orbital, i.e. this orbital consists mainly of atomic orbitals sited at the F atoms, which accommodate the extra electron; (2) the high electronegativity of the F ligands, which effectively supports strong bonding of an additional electron; (3) the large number of F ligands, which makes the effective delocalization (distribution) of the excess charge density over the large ligand sphere amenable; and (4) the high polarity (ionicity) of the M–F bonds [30]. A recent review article on multiply charged anions [34] gives a summary of fluoride molecules whose electron affinities are believed to be in excess of 5 eV. The first experimental photoelectron spectra of a superhalogen was recently reported by Wang et al. [35]. A large electron affinity should not, however, necessarily imply that the electron attachment cross section will be large. For example, UF_6 has a large electron affinity but a very small electron attachment rate for low energy electrons [36]. The electron attachment rate is a complex function of electronic- and nuclear wave functions overlap and the accompanying dynamics involving a breakdown of the Born-Oppenheimer approximation.

The large electron affinities of superhalogen molecules is expected to greatly influence the surface chemistry involving these species and thereby play a role in the yield of neutral hexafluorides. The production of metal hexafluorides by the reactions between metals and fluorine has a long history. In 1900, Moissan [37] reported that fluorine gas reacted vigorously with uranium metal to produce a volatile gas which was later identified as UF_6. In 1977, one of us

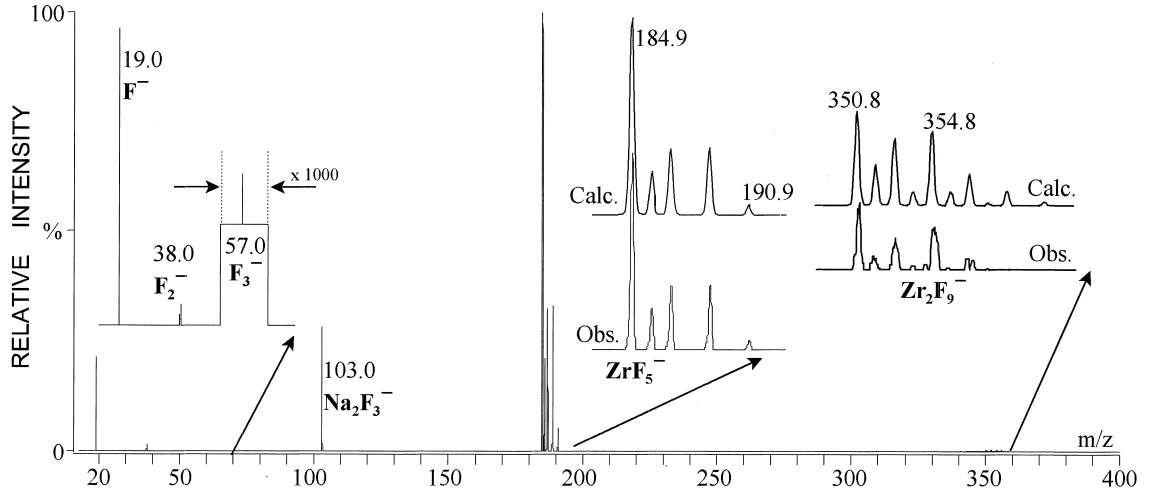

Fig. 10. The negative ion spectrum generated on resistively heating a Zr wire (127 μm × 4 mm) in a fluorine atmosphere (estimated 10^{-4} mbar within the ion source) within the ion source. The wire glowed cherry red. Insets are expanded regions of the spectrum comparing, where appropriate, the observed and calculated isotope clusters for the assigned elementary compositions.

showed that these reactions producing UF_6 also produced UF_6^- ions in great abundance [2]. Because the work function of clean uranium is low (~3.5 eV), it was speculated that negative ions of UF_6 were precursors to the yield of neutral UF_6. Since many hexafluoride molecules are prepared through burning metal in fluorine gas the production of negative ions is also expected to be important. This article reports a further more detailed study of the production of metal fluoride anions formed during the reactions between fluorine gas and hot metal filaments.

The negative ion spectra generated on resistively

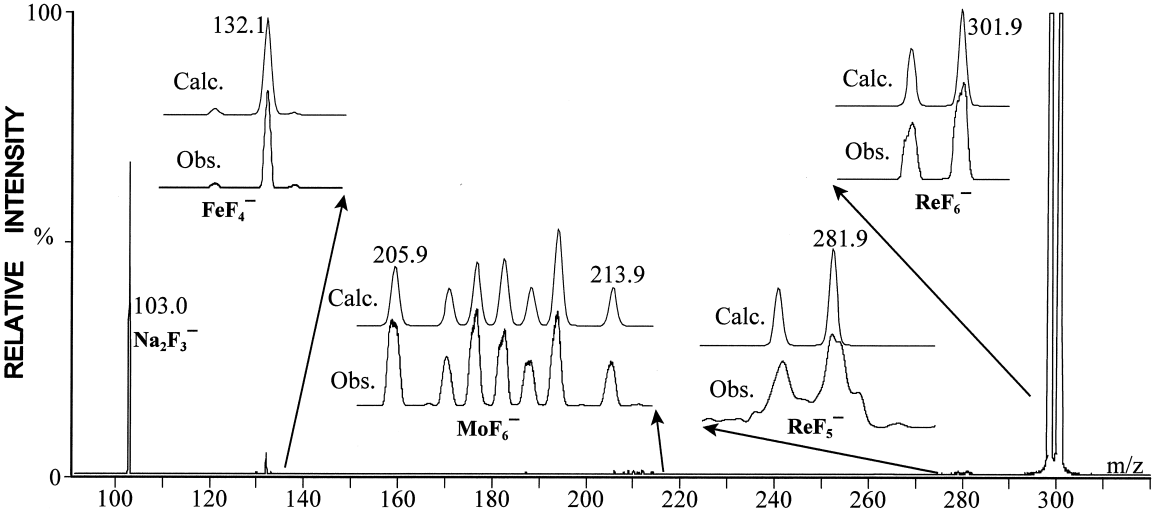

Fig. 11. The negative ion spectrum generated on resistively heating a Re wire (100 μm × 4 mm) in a fluorine atmosphere (estimated 10^{-4} mbar within the ion source) within the ion source. The wire glowed intensely white hot. Insets are expanded regions of the spectrum comparing, where appropriate, the observed and calculated isotope clusters for the assigned elementary compositions. The peaks at *m/z* 299/301 are overranged. The observed inset is taken from a spectrum recorded at a lower temperature.

Table 1
Anions observed on resistively heating various metal wires in a F_2 atmosphere within the ion source (see Figs. 10 and 11)

Wire metal/diam (μm)	Observed products[a]	Comments
Al/127	$Al_2F_7^-$	. . .
Au/250	AuF_2^- and AuF_3^-	ratio ~20/1
6/4 Au/Pd alloy/200	AuF_2^- and AuF_3^-	no PdF_x^- observed
Nb/250	NbF_6^-	. . .
Nichrom/250	. . .	no NiF_x^- or CrF_x^- observed
Pt/127	. . .	no PtF_x^- observed
Re/100	ReF_6^- and ReF_5^-	first ReF_6^-; ReF_5^- only on extensive heating (see Fig. 1)
Ta/250	TaF_6^-	. . .
Ti/127	TiF_5^- and TiF_4^-	first TiF_5^-; TiF_4^- only on extensive heating
V/127	VF_4^- and VF_5^-	first VF_4^-; VF_5^- only on extensive heating
W/76	WF_6^- and WF_5^-	first WF_6^-; WF_5^- only on further heating
Zr/127	ZrF_5^- and $Zr_2F_9^-$	these anions appear simultaniously (see Fig. 11)

[a] Products not associated with this specific metal (e.g. F_2^-, $Na_2F_3^-$, or FeF_4^-; see Figs. 10 and 11) not listed here.

heating Zr and Re wires in a fluorine atmosphere within the ion source of the mass spectrometer are displayed in Figs. 10 and 11, respectively. In Fig. 10, the isotope cluster at *m/z* 185 corresponds to that calculated for ZrF_5^-, thus establishing its identity. The same applies to the cluster starting at *m/z* 350, which corresponds to $Zr_2F_9^-$. (It should be noted that the relative intensities of the clusters displayed in the spectra represent only a "snapshot" of the progression of the reaction. For instance, the intensity ratio $Zr_2F_9^-/ZrF_5^-$ decreases as heating of the Zr wire within the source increases.) At the beginning of the analysis depicted in Fig. 10 this ratio is about 35%, whereas it is <1% at the time this snapshot (Fig. 10) was taken. Similar intensity variations as a function of time apply to Fig. 11 and to various other experiments as detailed in Table 1.

In Fig. 11 the appearance of clusters representing FeF_4^- and MoF_6^- are unexpected. They appear only toward the end of the analysis when the Re wire has attained white-hot temperatures. These same clusters also appear with other wire materials (e.g. W) having high melting points and thus the capability of substantially heating the ion source during the course of the reaction. Therefore, the iron and molybdenum generating these clusters are thought to derive from the stainless steel walls of the ion source upon extensive radiative- and convective heating by the glowing wire. Fluorides of Ni and Cr (other significant components of the 316 ss used to make the ion source) were not observed. This is consistent with the nonobservation of NiF_x^- and CrF_x^- when Nichrom wire was employed in the combustion (see Table 1).

It had been expected that gold and platinum would provide abundant peaks of AuF_6^- and PtF_6^- based on the very high electron affinities of the corresponding neutral molecules. As can be seen in Table 1, this was not the case. The nonobservation of AuF_6^- could be ascribed to a termination at the formation of the lower fluorides and AuF_6^- is not formed. However, since it is well known that PtF_6 is formed in fluorine/Pt combustion, we are at a loss to explain the absence of PtF_6^- in our experiments. The low energy electron attachment rate for PtF_6 may be very small, however the large electron affinity would assure that surface ionization would occur.

Besides the metal fluoride region of Fig. 10, two other areas are of interest; the low mass region (*m/z* 15–60) and the peak at *m/z* 103. The three lowest-mass peaks (*m/z* 19, 38, and 57) represent F^-, F_2^-, and F_3^-, respectively. Although F^- and F_2^- are observed in all the metal-wire/F_2 combustion analyses discussed here, F_3^- is seen only sporadically, and then only as a very weak peak. Its appearance does not seem to be

related to the type of metal wire under investigation, either with regard to longevity of the signal, or to signal intensity. In fact, F_3^- is more intense when the metal wire is dispensed with altogether, and an electron beam is introduced into the source while maintaining a relatively high fluorine gas pressure. It is only under these "electron capture" conditions of the experiment that *m/z* 57 had sufficient duration and abundance to be unambiguously identified as F_3^- by collision induced dissociation [38]. This was the first published observation of the gas-phase trifluoride anion reported in the literature.

A peak at *m/z* 103.0 ± .07 Da was previously observed on combustion of a gold wire in a fluorine atmosphere, and was tentatively ascribed [39] to AuF_6^{-3} on the basis of the observed mass (103 ± 1 Da) and the monoisotopic nature of the observed peak. One motivation for the present study was the verification (or otherwise) of that tentative assignment. [We note parenthetically that mass 103 was also observed in the LDNI MS of Na_3FeF_6 (see Fig. 7)]. The following observations are relevant to structural assignment of *m/z* 103.

(1) When using a gold wire in the combustion experiment (spectrum not illustrated) *m/z* 103 appears at the same mass as it does in Figs. 10 and 11, i.e. at *m/z* 103.0. The precision of mass assignments on the ZAB (see experimental) is significantly better than was possible on the TOF instrument (vintage 1970) used in the original observation. The presently observed mass of 103.0 ± 0.07 positively excludes AuF_6^{-3} (m/z_{calc} 103.652) as the proper assignment.

(2) The *m/z* 103 peak is seen in the fluorine atmosphere combustion of *all* of the metal wires examined in this study (see Table 1), independent of the metal employed. However, there is little consistency in the characteristics of the signal. It may be of long or short duration, and of high or low intensity. Even when all controllable experimental parameters are kept as constant as possible (i.e. metal type, wire diameter, fluorine pressure, heating current to the wire, etc.) the intensity and duration of the *m/z* 103 peak is unpredictable.

(3) Remaining candidates for assignment to the 103 peak are AlF_4^- and $Na_2F_3^-$ (each with $m/z_{calc.}$ 102.975, and therefore indistinguishable by the most accurate mass determination possible in this instrument configuration). If fortuitous traces of aluminum in the other wires, or in some component of the ion source, were responsible the genesis of *m/z* 103, then an abundance of aluminum in the form of pure Al wire used in the experiment would be expected to produce a superabundant and long-lived *m/z* 103 peak. This proved not to be the case and AlF_4^- is therefore excluded as the candidate.

(4) Na^+ is ubiquitous, and is the likely source for the production of $Na_2F_3^-$ in these experiments. This hypothesis is bolstered by the occasional observation of a minuscule peak at *m/z* 61.0 (probably corresponding to NaF_2^- generated on the wire). Furthermore, a modest increase in duration and intensity of *m/z* 103 peak is observed when the wire is intentionally doped with NaF solution prior to the experiment. Unfortunately, low energy collision induced dissociation [CID] experiments on this peak differ markedly from those obtained from similar precursor ions derived by electrospray ionization of NaF solutions. Whereas the *m/z* 103 peak derived from the electrospray experiment readily dissociates to *m/z* 61 (NaF_2^-, loss of NaF) on low energy collisions with Ar, no significant dissociation product was detected for the precursor derived from the 103 peak obtained by wire combustion.

The discussion previously presented concludes, by eliminating all other possibilities, that *m/z* 103 is $Na_2F_3^-$. The disparity of CID results on two different instrument types (BEqQ and QqQ) requires further comment however. The lack of a product–ion signal in the former experiment may be due to the difficulty experienced in tuning the instrument to observe the desired *m/z* 103 → 61 transition. The precursor ion must be decelerated from the operating energy of the magnetic sector (8 kV) to that of the quadrupole sector (~10 V). In addition, the ion energy within the analyzer quadrupole (Q) must be continuously adjusted as a function of product-ion mass to allow transmission of those product-ions. The transmission

efficiency through the qQ sector of a BEqQ instrument does not usually exceed 10%. Given the added difficulties of low intensity and uncertain duration of the precursor-ion in this case (i.e. *m/z* 103 from the burning of a wire in F_2) the product ion *m/z* 61 may simply have been "missed."

However, a second interesting possibility to account for the discrepancy in the "burning wire" (BEqQ) and electrospray (QqQ) CID results is that the structures of the $Na_2F_3^-$ precursor ions derived by these two methods are in fact different. Boldyrev (private communication) has performed calculations on linear ($D_{\infty h}$) and bipyramidal (D_{3h}) structures for $Na_2F_3^-$ with the result that the D_{3h} structure is predicted to be more stable by only ~0.6 kcal/mol. Both structures were found to be true minima. These two distinct isomeric structures would be expected to exhibit very different collisional dissociation patterns as observed. It is logical to propose that the linear $D_{\infty h}$ species would lose NaF upon collision, which is observed in the electrospray experiments. The filament reactions would then give rise to the more complicated D_{3h} species.

Several other metal wires aside from those depicted in Figs. 10 and 11 were subjected to combustion in the presence of F_2. The results are summarized in Table 1. The observation of $ReF_{5,6}^-$ can be attributed to low energy electron attachment to ReF_6 on the surface. Both of these ions are seen in low energy electron attachment experiments [40]. Since the electron affinity of ReF_6 is >5.0 eV, surface ionization is also possible. Perhaps the most striking result of this study is the nonobservation of PtF_6^-. To our knowledge, electron attachment studies for this molecule have not been performed, however, the electron affinity for PtF_6 is believed to be >9.3 eV [29] and one would expect that PtF_6^- would have been produced by surface ionization.

4. Conclusions

In summary, a wide variety of negative ions have been produced on surfaces heated via lasers or from combusting wires. We have attempted to delineate the processes occurring on the surface as either "free" electron attachment or surface ionization. For many of the laser experiments (e.g. $C_{60}H_{36}$) thermal electron attachment is believed to be occurring. However, the laser can play a role in the production or photodissociation of the anions observed. For the case of UF_6 reported earlier [2] surface ionization is occurring exclusively since UF_6 does not attach thermal electrons [36]. Although slow electrons do not attach to UF_6, it is well known that UF_6 can charge exchange with ions such as SF_6^- to form UF_6^-. Thus we suggest that some of the ions observed herein are a result of "quasifree" electron attachment. A filament has electrons occupying the metal band structure up to the Fermi level. As the filament is heated the Fermi edge is "blurred" giving rise to electrons up to and beyond (thermionic emission) the ionization limit. Those electrons with energies insufficient to overcome their image charge attraction are available for attachment (i.e. "charge transfer") to molecules on the surface. We are attempting to distinguish "free electron" attachment with "charge exchange" between the surface and the molecule. Laser heating of the surface provides the kinetic energy necessary for the ions to escape the surface.

The mechanism discussed above evoking quasifree electron attachment may have relevance to recent experiments involving electron-stimulated desorption of Cl^- from surfaces containing CCl_2F_2 and water or ammonia at cryogenic temperatures [41]. In these experiments the Cl^- yield produced by dissociative electron attachment to a monolayer of CCl_2F_2 is enhanced by factors of 10^2–10^4 when water or ammonia are present on the Ru surface. We propose that this enhancement is due to electrons which are self trapped to dipole states of water or ammonia. These weakly bound electrons are then free to migrate through the dipole states which constitutes a type of band structure becoming localized on the CCl_2F_2 to produce Cl^-. Although the dipole moments of water and ammonia are too small to allow bound states in the gas phase as a result of rotation of the free molecule, the surface acts to lock-in the dipole permitting the formation of a diffuse dipole anion (for a review of dipole bound anions see [42] and [43]).

Negative ion formation on surfaces is clearly a complicated subject. In this study, we have attempted to relate those processes which are known to occur in the gas phase to those observed in the experiments described herein.

Acknowledgements

This research was supported by the National Science Foundation (CHE-9981945). One of the authors (A.S.L.) would like to acknowledge financial support from the Appalachian Colleges Association (ACA). The authors thank to T. Free and E. French for construction of the ZAB ion source and the floated high amperage power supply, respectively.

References

[1] J.B. Hasted, Physics of Atomic Collisions, Elsevier, New York, 1972, p. 276.
[2] R.N. Compton, P.W. Reinhardt, W.R. Garrett, J. Chem. Phys. 66 (1977) 4712.
[3] L. Sanche, Scan. Microsc. 9 (1995) 619.
[4] L. Zhou, A.A. Tuinman, R.N. Compton, A.S. Lahamer, Electrochem. Soc. Proc. 98 (1998) 493.
[5] R.L. Hettich, C. Jin, P.F. Britt, A.A. Tuinman, R.N. Compton, Mater. Res. Soc. Symp. Proc. 349 (1994) 133.
[6] A.D. Darwish, A.K. Abdul-Sada, G.J. Langley, H.W. Kroto, R. Taylor, D.R.M. Walton, J. Chem. Soc. Perkin Trans. 2 (1995) 2359.
[7] A.A. Gakh, A.A. Tuinman, J.L. Adcock, R.A. Sachleben, R.N. Compton. J. Am. Chem. Soc. 116 (1994) 819.
[8] Y. Chai, T. Guu, C. Lin, R.E. Haufler, L.P.F. Chibatnte, J. Fure, L. Wang, J.M. Alford, R.E. Smalley, J. Phys. Chem. 95 (1991) 7564.
[9] A.S. Lahamer, Z.C. Ying, R.E. Haufler, R.L. Hettich, R.N. Compton, Adv. Metal Semicond. Clusters 4, (1989) 179.
[10] M. Lezius, T.D. Mark, Chem. Phys. Lett. 203 (1993) 232; M. Lezius, P. Scheier, M. Foltin, B. Dunser, T. Rauth, V.M. Kratchmer, T.D. Mark, Int. J. Mass Spectrom. Ion Processes 129 (1993) 49.
[11] T. Jaffke, E. Illenberger, E. Lezius, S. Matejcik, D. Smith, T.D. Mark, Chem. Phys. Lett. 26 (1995) 213.
[12] S. Matejcik, T.D. Mark, P. Spanel, D. Smith, T. Jaffke, E. Illenberger, J. Chem. Phys. 102 (1995) 2516.
[13] J. Huang, H.S. Carman Jr., R.N. Compton, J. Phys. Chem. 99 (1995) 1719.
[14] D. Smith, P. Spanel, T.D. Mark, Chem. Phys. Lett. 213 (1993) 202; P. Spanel, D. Smith, Chem. Phys. Lett. 29 (1994) 262.
[15] E. Tosatti, N. Manini, Phys. Lett. 203 (1994) 232.
[16] Y.V. Vasil'ev, R.F. Tuktarov, V.A. Mazunov, Rapid Commun. Mass. Spectrom. 11 (1997) 757.
[17] O. Elhamidi, J. Pommier, R. Abouaf, J. Phys. B: At. Mol. Opt. Phys. 30 (1997) 4633.
[18] G.J. Schulz, J. Appl. Phys. 31 (1960) 1134.
[19] L.G. Christophorou, R.N. Compton, G.S. Hurst, P.W. Reinhardt, J. Chem. Phys. 43 (1965) 4273.
[20] R.N. Compton, R.H. Huebner, P.W. Reinhardt, L.G. Christophorou, J. Chem. Phys. 48 (1968) 901.
[21] J.M. Weber, M.-W. Rouf, H. Hotop, Z. Phys. D 37 (1996) 351.
[22] C.D. Finch, R.A. Popple, P. Nordlander, F.B. Dunning, Chem. Phys. Lett. 244 (1995) 345.
[23] H.S. Carman Jr., R.N. Compton, J. Chem. Phys. 98 (1993) 2473.
[24] Proceedings of the Sixth International Symposium on the Production and Neutralization of Negative Ions and Beams, A. Herschcovitch, J.G. Alessi (Eds.), AIP, New York, 1992.
[25] The LEAR Team, IEEE Trans. Nucl Sci. NS-32 (1985) 2652; R. Gianniui, Proc. Eur. Part. Accel. Conf. Rome 1 (1988) 505.
[26] S.L. Kramer, R.L. Martin, IEEE Trans. Nucl. Sci. NS-32 (1985) 3311; R.L. Martin, Nucl. Instrum. Methods, Phys. Res. B. 24/25 (1987) 1089; 40/41 (1989) 1331; G. Arduini et al., Nucl. Instrum. Methods Phys. Res. A. 365 (1995) 542.
[27] D.A. Gray, IEEE Trans. Nucl. Sci. NS-32 (1985) 2638; G.H. Ress, Proc. IEEE Part. Accel. Conf., Washington 1 (1987) 830.
[28] G.I. Dinov, Rev. Sci. Instrum. 67 (1996) 3393.
[29] N. Bartlett, Angew. Chem. Int. Ed. Engl. 7 (1968) 433.
[30] R.N. Compton, P.W. Reinhardt, C.D. Cooper, J. Chem. Phys. 68 (1978) 2023.
[31] L.N. Sidorov, Usp. Khim. 51 (1982) 625; Int. J. Mass Spectrom. Ion Phys. 39 (1981) 311.
[32] G.L. Gutsey, A.I. Bolderev, Chem. Phys. Lett. 101 (1983) 441.
[33] R.N. Compton, P.W. Reinhardt, J. Chem. Phys. 72 (1980) 4655.
[34] M.K. Scheller, R.N. Compton, L.S. Cederbaum, Science 270 (1995) 1160.
[35] X.B. Wang, C.F. Ding, L.S. Wang, A.I. Bolderev, J. Simons, J. Chem. Phys. 110 (1999) 4763.
[36] R.N. Compton, J. Chem. Phys. 66 (1977) 4478.
[37] H. Moissan, in Le Fluor, Steinheil, Paris, 1900.
[38] A.A. Tuinman, A.A. Gakh, R.L. Hinde, R.N. Compton, J. Am. Chem. Soc. 121 (1999) 8397.
[39] R.N. Compton, in Photophysics and Photochemistry in the Vacuum Ultraviolet, S.P. McGlynn et al. (Eds.), Reidel, Dordrecht, 1985, p. 261.
[40] J.A.D. Stockdale, R.N. Compton, H.C. Schweinler, J. Chem. Phys. 53 (1970) 1502.
[41] Q.-B. Lu, T.E. Madey, Phys. Rev. Lett. 82 (1999) 4122; J. Chem. Phys. 111 (1999) 2861.
[42] C. Desfrancois, H. Abddoul-Carmine, J.-P. Schermann, Int. J. Mod. Phys. B 10 (1996) 1339.
[43] R.N. Compton, in The Role of Rydberg States in Spectroscopy and Photochemistry, C. Sandorfy (Ed.), Kluwer, Dordrecht 1999.